Supplementary Information

Over 28% Efficiency Perovskite/Cu(InGa)Se_2 Tandem Solar Cells: Highly Efficient Sub-cells and Their Bandgap Matching

Xinxing Liu,‡[1] Junjun Zhang,‡[1] Liting Tang,‡[1] Junbo Gong,‡[1]* Wang Li,[1] Zengyang Ma,[1] Zexin Tu,[1] Yanyan Li,[1] Ruiming Li,[1] Xuzhi Hu,[1] Chen Shen,[1] He Wang,[2] Zhiping Wang,[1] Qianqian Lin,[1] Guojia Fang,[1] Sheng Wang,[1] Chang Liu,[1] Zengming Zhang,[2] Jianmin Li,[1]* Xudong Xiao[1]*

1. School of Physics and Technology, and Key Laboratory of Artificial Micro- and Nano-structures of Ministry of Education, Wuhan University, Wuhan 430072, China.

2. The Center for Physical Experiments, School of Physics Science, University of Science and Technology of China, Hefei 230026, China

‡These authors contributed equally.

Corresponding authors: Junbo Gong (gongjunbo@whu.edu.cn), Jianmin Li (ljmphy@whu.edu.cn), Xudong Xiao (xdxiao@whu.edu.cn)

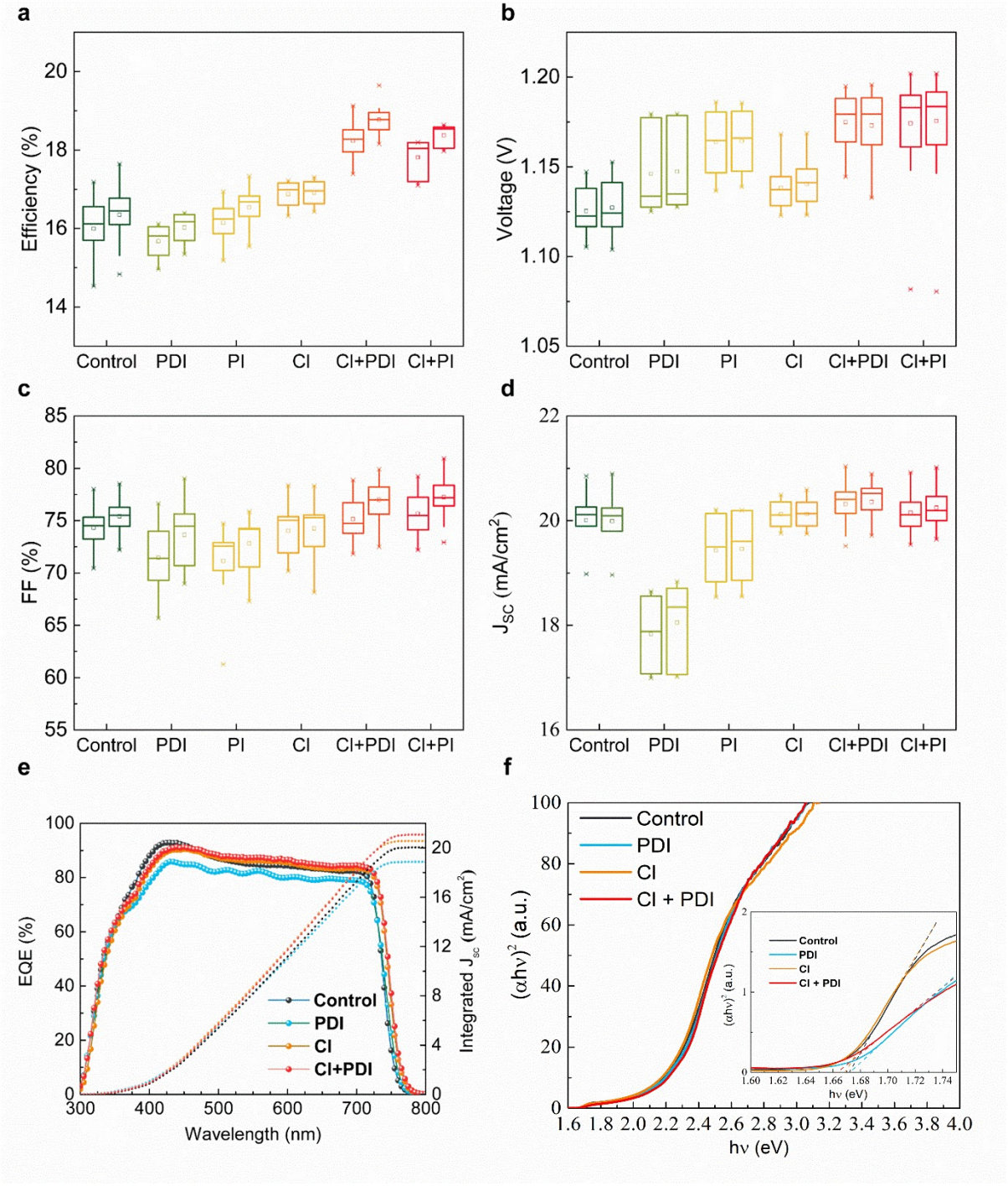

Supplementary Figure 1. Comparison of PI and PDI surface treatments. a-d, Statistical boxplot of PCE (**a**), V_{oc} (**b**), *FF* (**c**) and J_{sc} (**d**) for six groups of PSC samples: **Control**, **PDI**, **PI**, **CI**, **CI+PDI**, and **CI+PI**. The mean value, maximum and minimum values, and 25%-75% region of data was represented by the open circle, top and bottom bars, and rectangle, respectively. Unlike the work by Li *et al.*,[1] who discovered that PI is better than PDI to passivate the surface of normal bandgap perovskite films, in this work, we found PDI is better than PI to boost the performance of wide bandgap perovskite solar cells. **e**, The *EQE* spectra

and the corresponding integrated J_{sc} of the representative devices from **Control**, **PDI**, **Cl**, and **Cl+PDI** groups. **f**, Absorption spectra of the representative perovskite films from **Control**, **PDI**, **Cl**, and **Cl+PDI** groups.

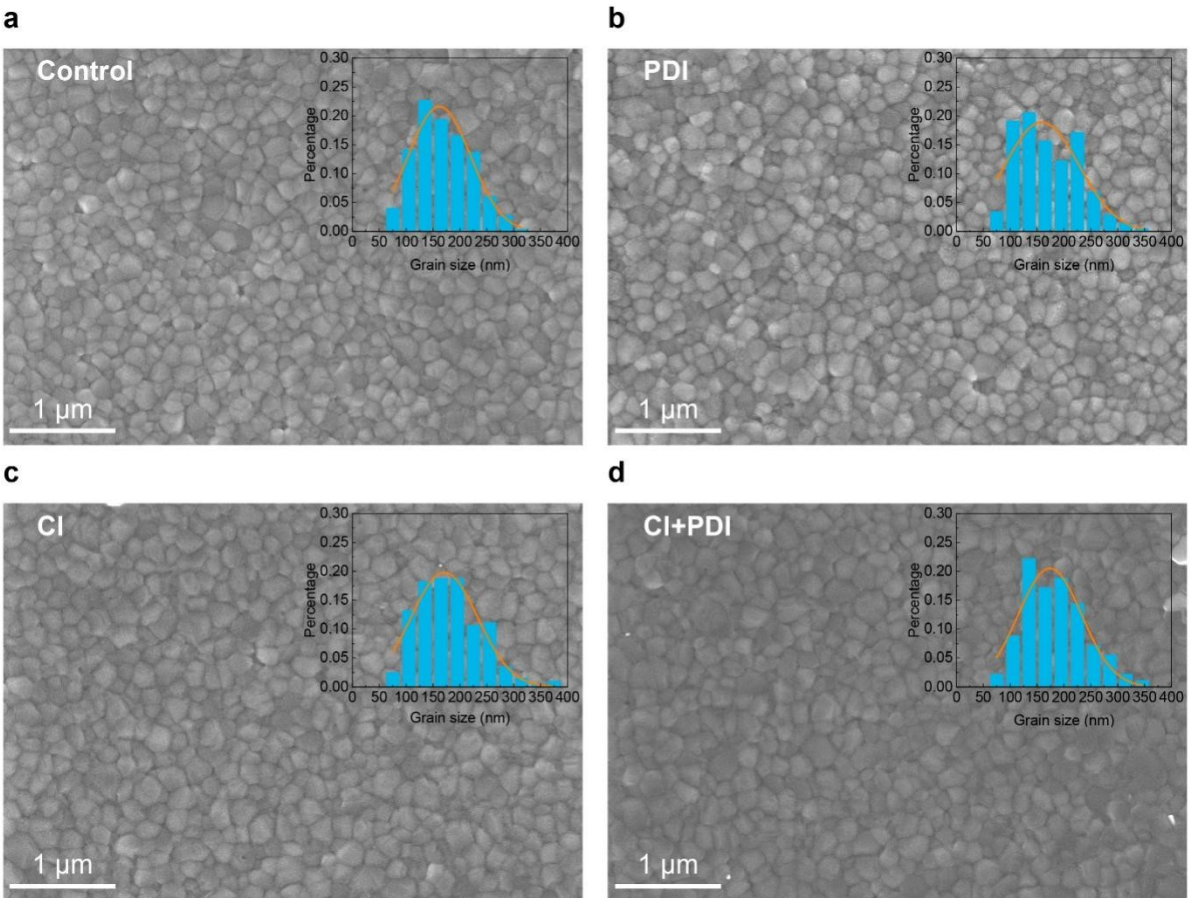

Supplementary Figure 2. Film morphology and grain statistics. Top view SEM images of representative perovskite films from the four groups: **a**, **Control**, **b, PDI**, **c, Cl**, **d, Cl+PDI.** The insets in the respective images show the statistics of the grain size distribution.

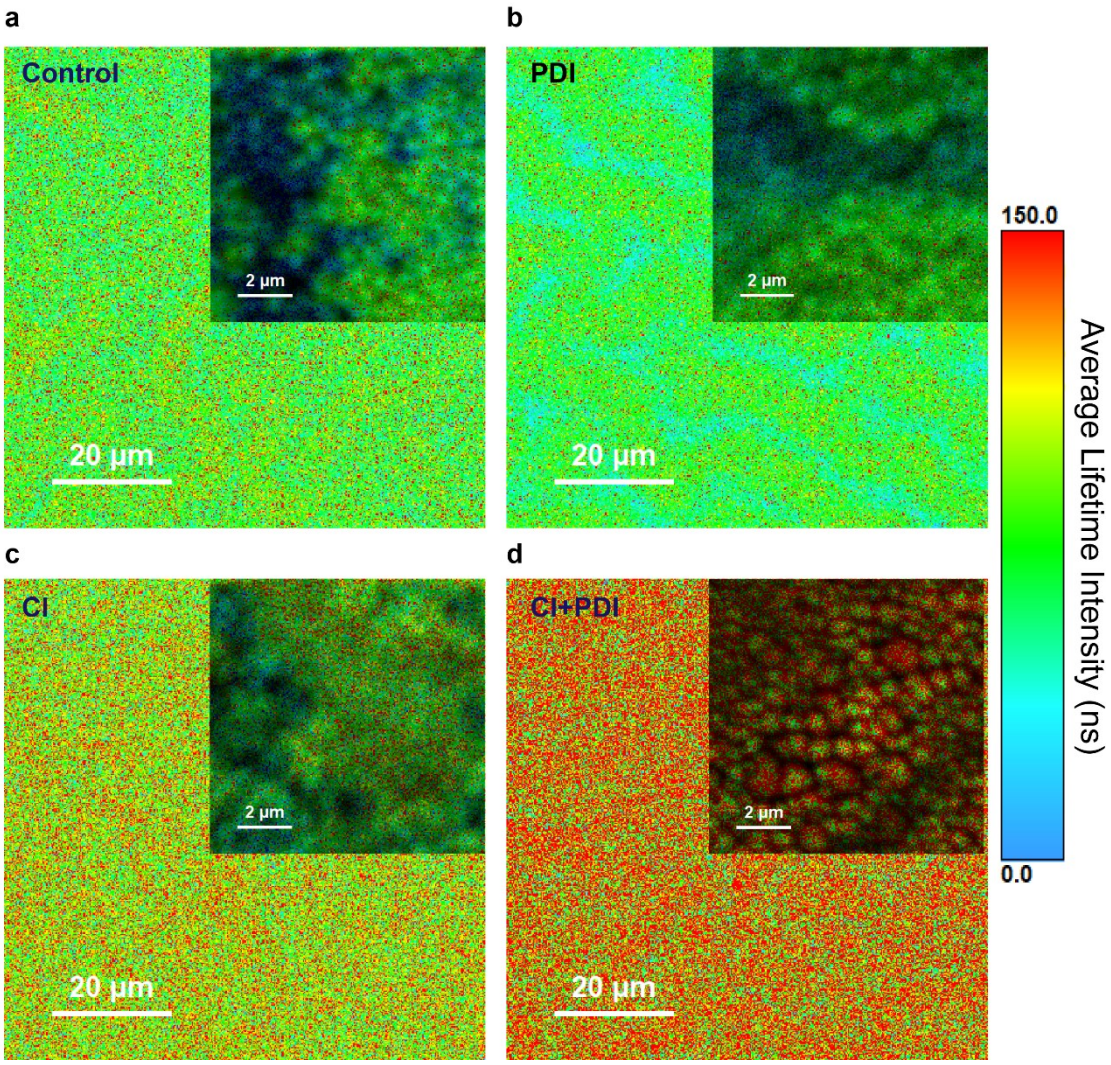

Supplementary Figure 3. Uniformity of fluorescence lifetime images. **a-d,** Fluorescence lifetime image microscopy of representative perovskite films from the four groups. Insets are the corresponding zoom-in images.

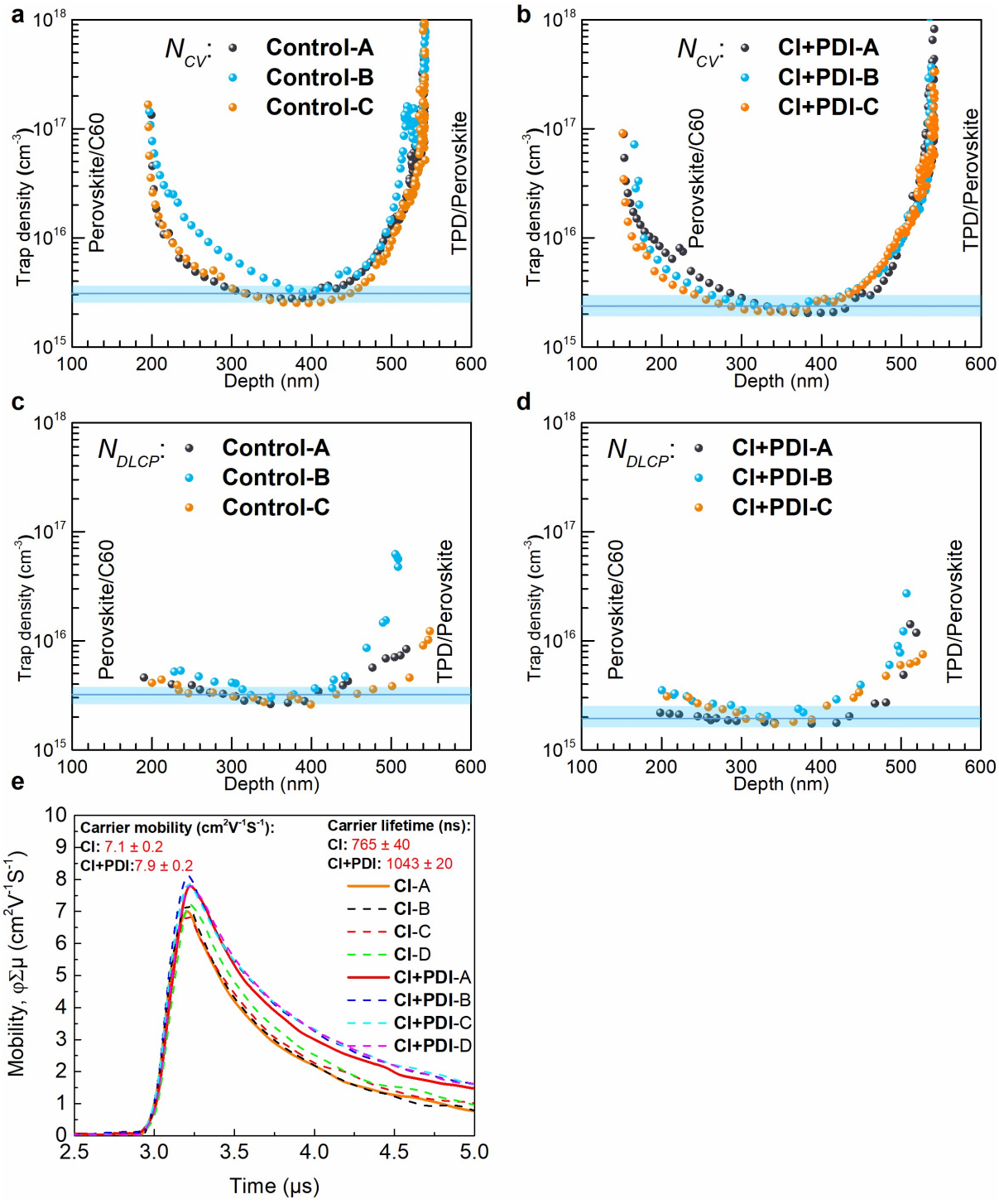

Supplementary Figure 4. Reproducibility measurement for defect passivation effect. a-b, CV profiling for **Control** and **Cl+PDI**. **c-d**, DLCP profiling for **Control** and **Cl+PDI**. **e**, Photoconductivity transients measured by TRMC for **Cl** and **Cl+PDI**.

a

	n	J_0 (mA·cm^{-2})	R_S (Ω·cm^2)	R_{SH} (Ω·cm^2)
Control	1.36	1.88E-7	0.63	1360
PDI	1.43	2.49E-7	1.47	903
CI	1.26	3.80E-8	0.93	9760
CI+PDI	1.23	1.44E-8	0.65	3190

b

	n	J_0 (mA·cm^{-2})	R_S (Ω·cm^2)	R_{SH} (Ω·cm^2)
Control	1.24	2.98E-8	1.31	377
PDI	1.52	6.98E-7	1.59	60
CI	1.20	2.36E-8	1.10	1630
CI+PDI	1.13	3.89E-9	1.17	3420

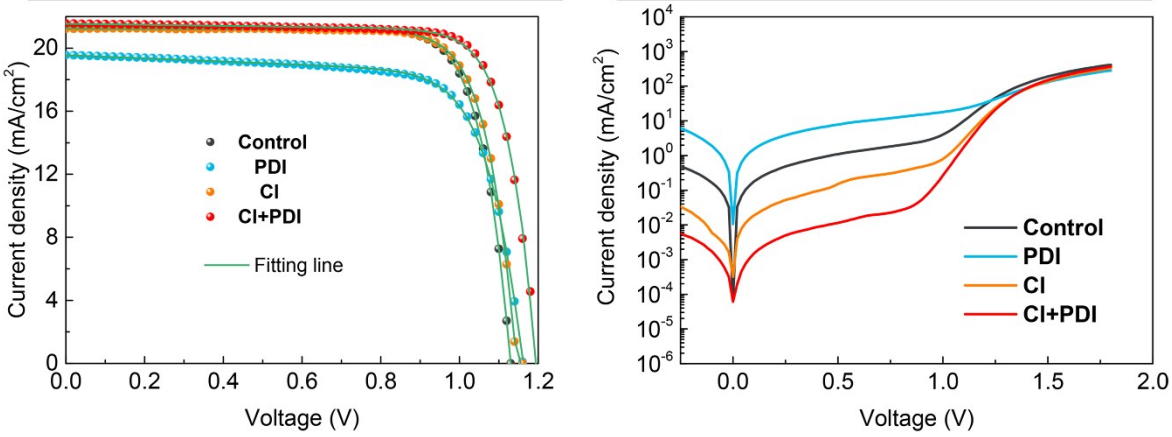

Supplementary Figure 5. Deduction of diode reverse saturation current density J_0. The *J-V* curves measured under (**a**) AM 1.5G light illumination and (**b**) in dark respectively. The J_0 values were obtained by fitting the J-V curves with $J = J_L - J_0\left[exp\left(\frac{V+JR_s}{nkT}\right) - 1\right] - \frac{V+JR_s}{R_{sh}}$.

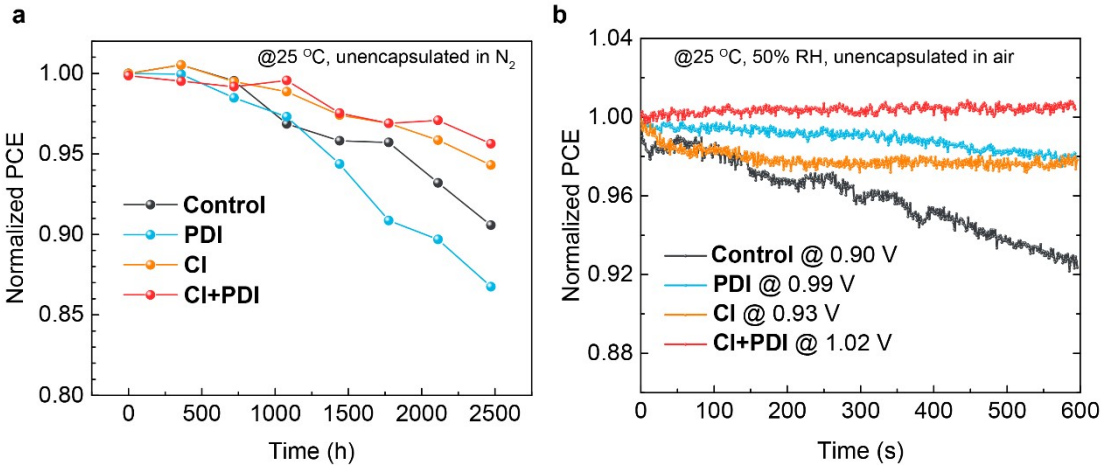

Supplementary Figure 6. Device stability test. a, The long-term storage stability in N_2 atmosphere. **b**, The steady power output (SPO) under 1-sun illumination measured at 25°C, 50% RH in air for 10 minutes.

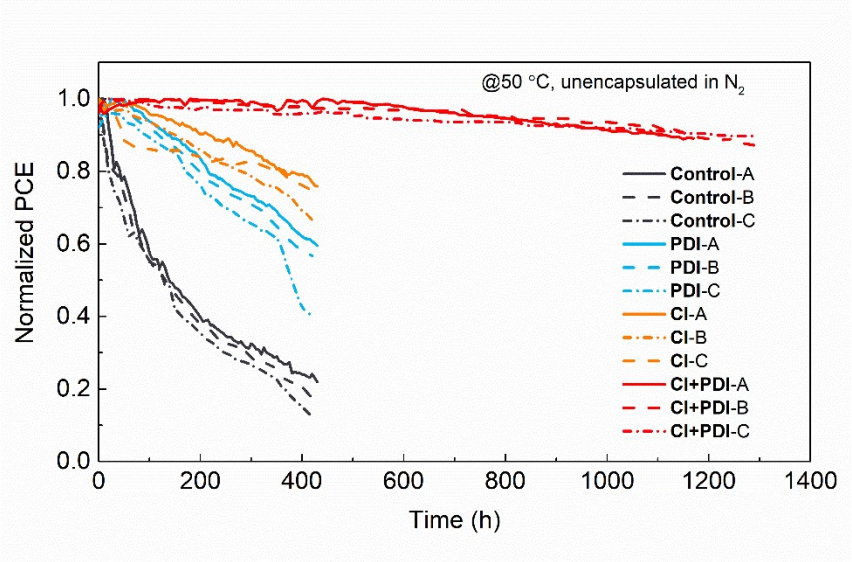

Supplementary Figure 7. Reproducibility measurement for device stability. Operational stability of devices from the four groups under MPP tracking with continuous illumination at 50 °C in N_2 atmosphere.

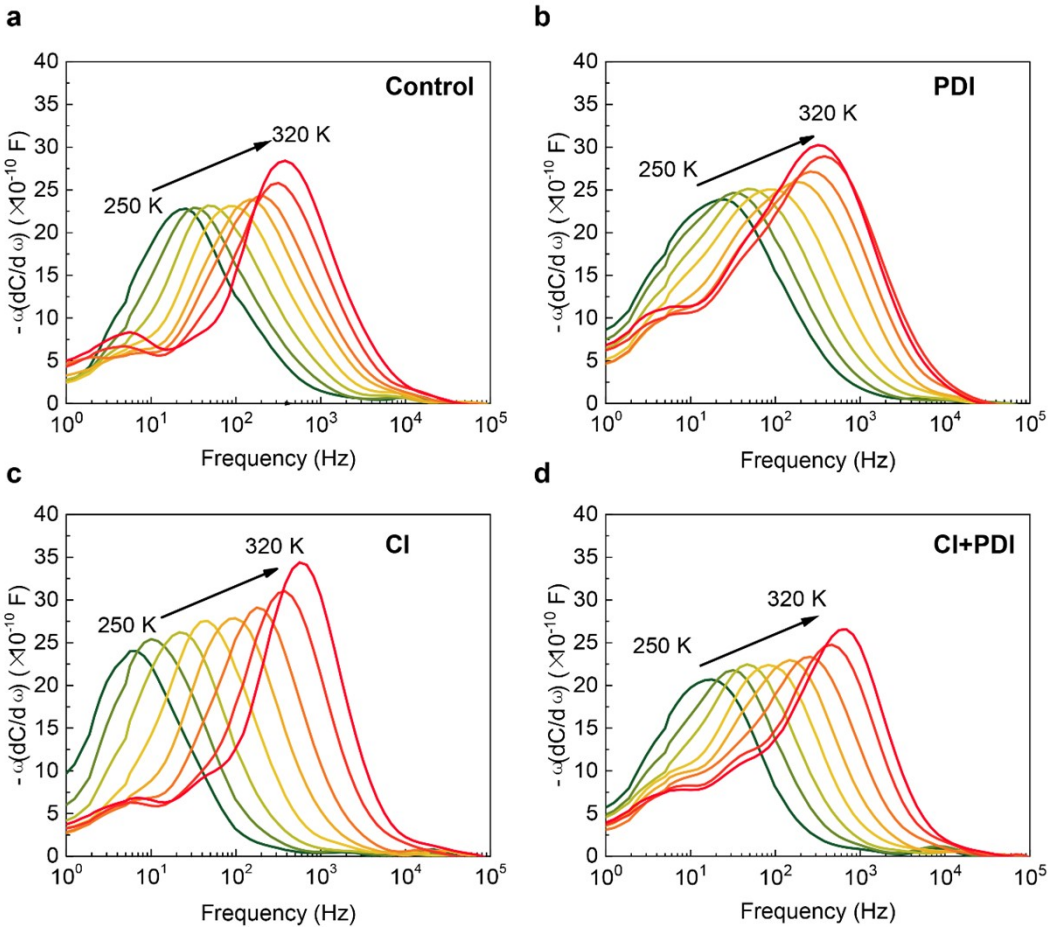

Supplementary Figure 8. Thermal admittance spectroscopy. Plot of $-\omega dC/d\omega$ vs frequency at various temperatures: **a**, **Control** device, **b**, **PDI** device, **c**, **Cl** device, and **d**, **Cl+PDI** device.

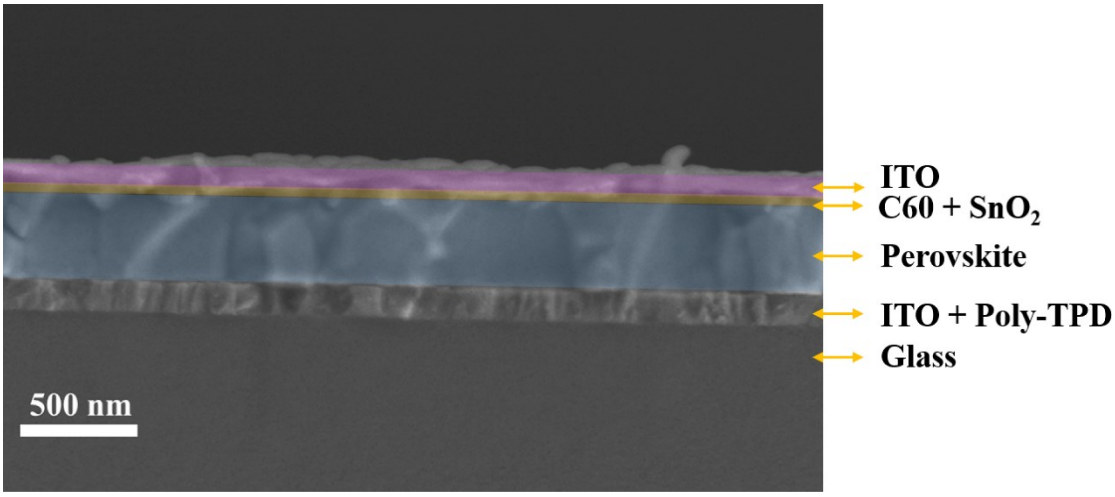

Supplementary Figure 9. Structure of a semi-transparent perovskite solar cell. Different color code in the cross-sectional SEM image labeled different layers of materials in the device.

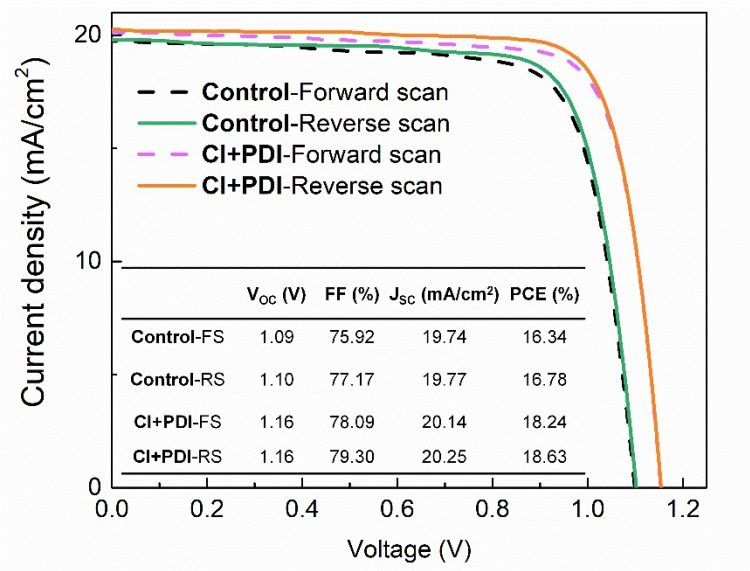

Supplementary Figure. 10. The effect of Cl incorporation and PDI treatment on ST-PSC devices. Comparison of ST-PSC devices before and after perovskite optimization.

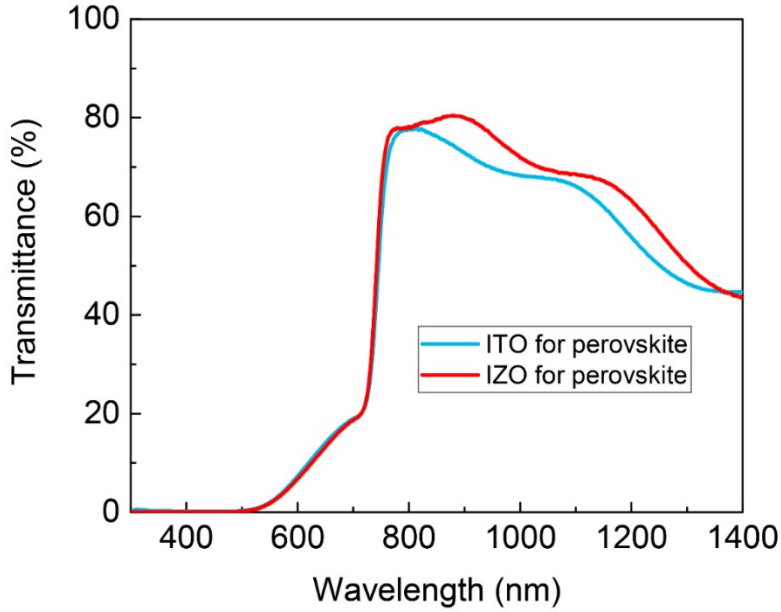

Supplementary Figure 11. Transmittance spectra in air. Two spectra of the highly efficient semitransparent perovskite solar cells with either ITO or IZO as the contact electrodes. The PSC-IZO clearly showed a better transmittance in the infrared region.

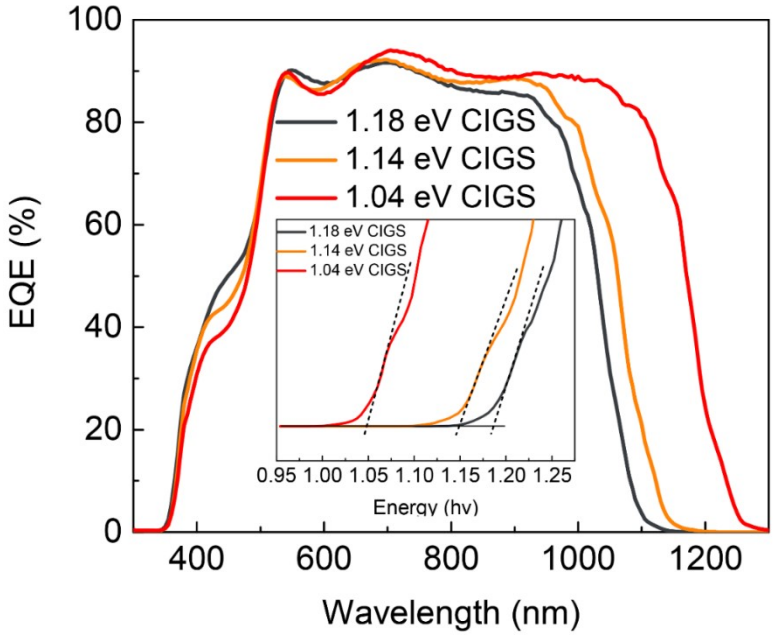

Supplementary Figure 12. Comparison of EQE spectra. The EQE spectra of CIGS solar cells with different bandgaps. The inset showed the edges of the long wavelength response, from which the bandgap of CIGS could be evaluated.

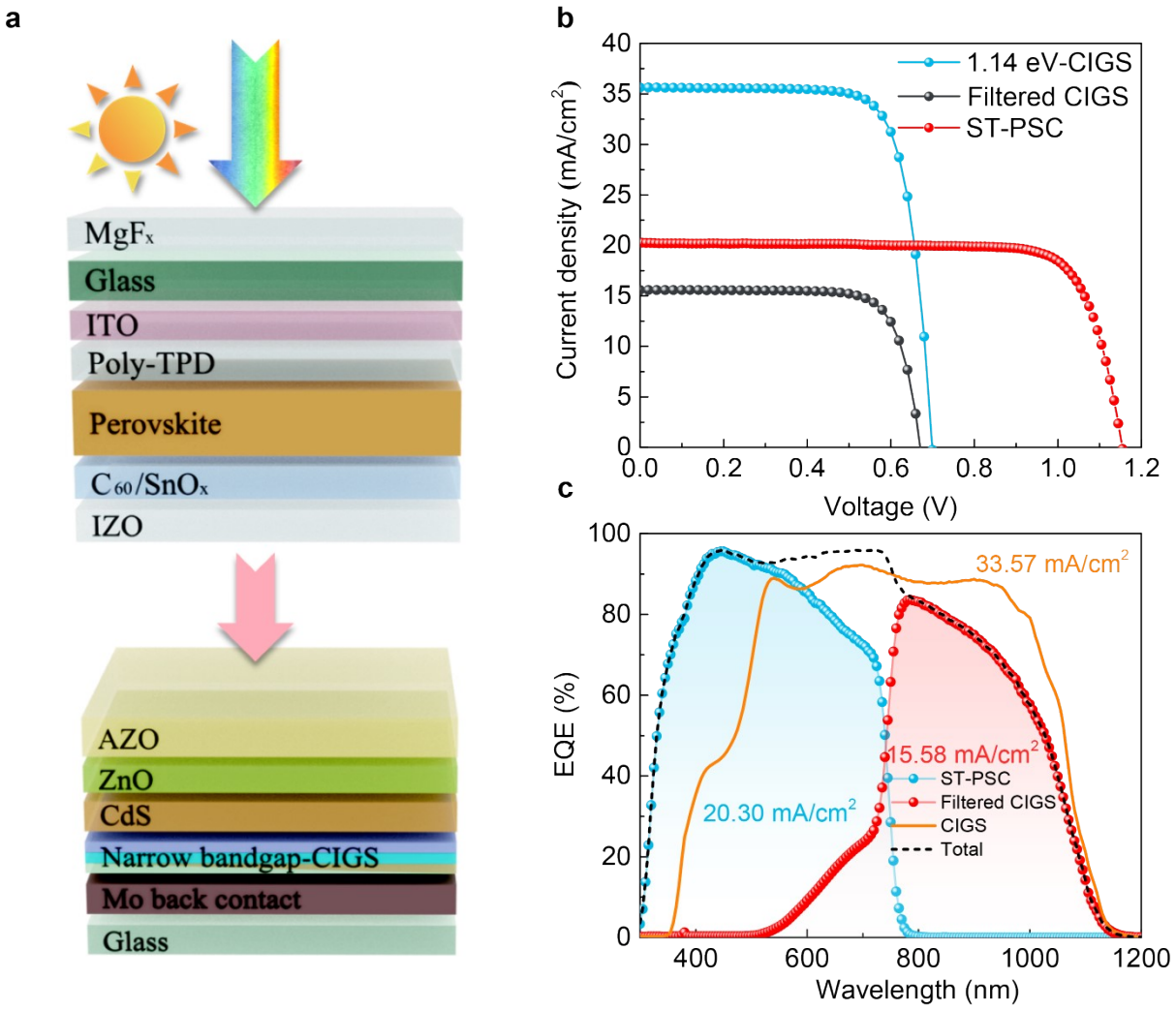

Supplementary Figure 13. a, Schematic of the 4-T PSC/CIGS tandem solar cell. Index matching fluid was applied between the two sub-cells to reduce reflection therein. **b**, Current density-voltage curves based on 1.14 eV-CIGS, **c**, EQE spectra of the tandem cell based on 1.14 eV-CIGS.

Supplementary Table 1. Carrier lifetime measured by TRPL decay curves. The fitting parameters with a bi-exponential decay equation are listed below.

	A_1	τ_1 (ns)	A_2	τ_2 (ns)	τ_{vag} (ns)
Control	48%	35	52%	122	80
PDI	32%	41	68%	83	69
Cl	52%	49	48%	172	108
Cl + PDI	21%	73	79%	255	216

Supplementary Table 2. Summary of semi-transparent PSCs. Photovoltaic parameters of semi-transparent PSCs reported in recent years. * marked the certified results.

Year[ref]	Bandgap (eV)	Configuration	Current density (mA/cm^2)	Voltage (V)	FF (%)	PCE (%)
2017[2]	1.73	TiO_2/Perovskite/ PTAA/MoOx/ITO	19.4	1.12	73.0	15.9
2018[3]	1.55	CuSCN/Perovskite/ PCBM/ ZnO:Al-NP/AgNW	21.0	1.01	74.1	17.1
2018[4]	1.72	SnO_2/Perovskite/ Spiro-OMeTAD/ MoO_x/ITO	15.4	1.22	73.4	13.8
2019[5]	1.68	ITO/PTAA/ Perovskite/C_{60}/ SnO_x/Zn:SnO_x (ZTO)/IZO	19.6	1.14	76.8	17.1
2019[6]	1.67	ITO/PolyTPD/ Perovskite/LiF/C_{60}/ SnO/ZTO/ITO	19.1	1.21	80.2	18.6
2019[7]	1.72	ITO/TiO_2/Perovskite/ Spiro-MeOTAD/ MoO_x/IZO	18.0	1.21	78.9	17.1
2019[8]	1.55	ITO/NiO_x/Perovskite/ PCBM/ZnO-NP/ BCP/IZRO	19.8	1.01	78.0	15.6
2020[9]	1.63	IZrO/SnO_2/Perovskite /Spiro-OMeTAD/ MoO_3/IZO/MgF_2	22.3	1.12	77.7	19.4
2020[10]	1.55	TiO_2/Perovskite/ Spiro-OMeTAD/ Au/MoO_x	19.8	1.16	79.9	18.3
2021[11]	1.50	ITO/SnO_2/Perovskite/ Spiro-OMeTAD/ Cr/Au/MgF_2	21.9	1.13	79.7	19.8
2022[12]	1.75	FTO/SnO_2/Perovskite/ Spiro-OMeTAD/ Au/MoO_x/ITO	17.53	1.21	80.1	17.0
2022[13]	1.77	ITO/SnO_2/Perovskite/ Spiro-OMeTAD/ MoO_x/IZO/MgF_2	18.8	1.24	79.6	18.6
2022[14]	1.60	ITO/PTAA/Perovskite /PCBM/ZnO/ITO	22.2	1.11	71.4	17.6

2022[15]	1.65	SnO_2/Perovskite/ Spiro-OMeTAD/ MoO_x / ITO	19.6	1.23	78.7	18.9
This work*	1.67	ITO/Poly-TPD/ Perovskite/C_{60}/SnO_x/ IZO	19.0	1.20	82.9	18.7

Supplementary Note 1. Certified performance of a Cl + PDI opaque device after stored at N_2 atmosphere for 92 days. This opaque PSC device with PCE of 19.7% (V_{oc} = 1.192 V, J_{sc} = 20.73 mA/cm^2, FF = 79.59%) measured in house was sent to Shanghai Institute of Microsystem and Information Technology, Chinese Academy of Science for third party certification. The certified PCE of 20.0% (V_{oc} = 1.205 V, J_{sc} = 20.92 mA/cm^2, FF = 79.51%) was obtained.

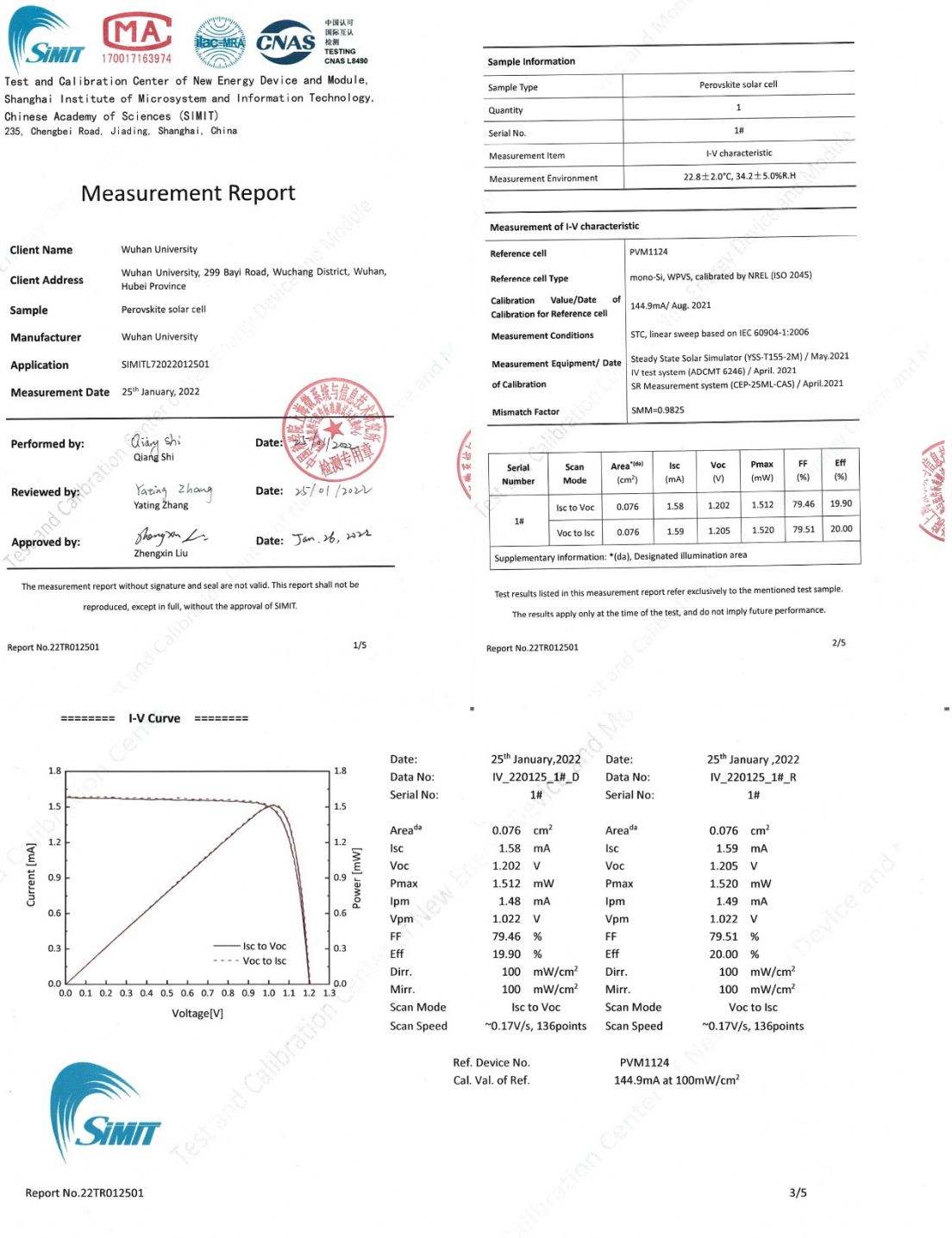

Test and Calibration Center of New Energy Device and Module,
Shanghai Institute of Microsystem and Information Technology,
Chinese Academy of Sciences (SIMIT)
235, Chengbei Road, Jiading, Shanghai, China

Measurement Report

Client Name	Wuhan University
Client Address	Wuhan University, 299 Bayi Road, Wuchang District, Wuhan, Hubei Province
Sample	Perovskite solar cell
Manufacturer	Wuhan University
Application	SIMITL72022012501
Measurement Date	25th January, 2022

Performed by: Qiang Shi Date: 25/01/2022
Reviewed by: Yating Zhang Date: 26/01/2022
Approved by: Zhengxin Liu Date: Jan. 26, 2022

The measurement report without signature and seal are not valid. This report shall not be reproduced, except in full, without the approval of SIMIT.

Report No.22TR012501 1/5

Sample Information	
Sample Type	Perovskite solar cell
Quantity	1
Serial No.	1#
Measurement Item	I-V characteristic
Measurement Environment	22.8±2.0°C, 34.2±5.0%R.H

Measurement of I-V characteristic	
Reference cell	PVM1124
Reference cell Type	mono-Si, WPVS, calibrated by NREL (ISO 2045)
Calibration Value/Date of Calibration for Reference cell	144.9mA/ Aug. 2021
Measurement Conditions	STC, linear sweep based on IEC 60904-1:2006
Measurement Equipment/ Date of Calibration	Steady State Solar Simulator (YSS-T155-2M) / May.2021 IV test system (ADCMT 6246) / April. 2021 SR Measurement system (CEP-25ML-CAS) / April.2021
Mismatch Factor	SMM=0.9825

Serial Number	Scan Mode	Area*(da) (cm^2)	Isc (mA)	Voc (V)	Pmax (mW)	FF (%)	Eff (%)
1#	Isc to Voc	0.076	1.58	1.202	1.512	79.46	19.90
	Voc to Isc	0.076	1.59	1.205	1.520	79.51	20.00

Supplementary Information: *(da), Designated illumination area

Test results listed in this measurement report refer exclusively to the mentioned test sample.
The results apply only at the time of the test, and do not imply future performance.

Report No.22TR012501 2/5

======== I-V Curve ========

Date:	25th January,2022		Date:	25th January ,2022	
Data No:	IV_220125_1#_D		Data No:	IV_220125_1#_R	
Serial No:	1#		Serial No:	1#	
Area[da]	0.076	cm^2	Area[da]	0.076	cm^2
Isc	1.58	mA	Isc	1.59	mA
Voc	1.202	V	Voc	1.205	V
Pmax	1.512	mW	Pmax	1.520	mW
Ipm	1.48	mA	Ipm	1.49	mA
Vpm	1.022	V	Vpm	1.022	V
FF	79.46	%	FF	79.51	%
Eff	19.90	%	Eff	20.00	%
Dirr.	100	mW/cm^2	Dirr.	100	mW/cm^2
Mirr.	100	mW/cm^2	Mirr.	100	mW/cm^2
Scan Mode	Isc to Voc		Scan Mode	Voc to Isc	
Scan Speed	~0.17V/s, 136points		Scan Speed	~0.17V/s, 136points	

Ref. Device No. PVM1124
Cal. Val. of Ref. 144.9mA at 100mW/cm^2

Report No.22TR012501 3/5

======== **Normalized External Quantum Efficiency Curve** ========

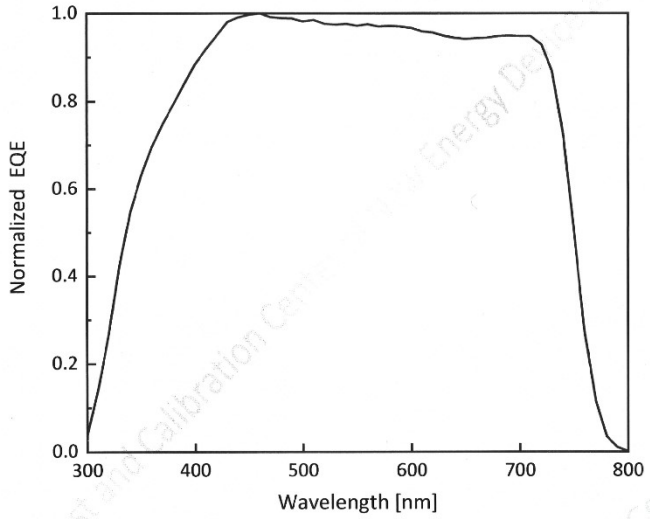

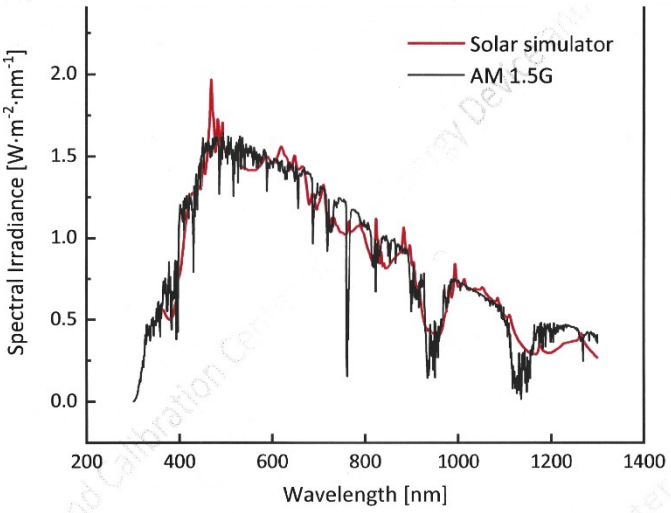

------- End of Report -------

Supplementary Note 2. The certification report for a semi-transparent PSC (ST-PSC). Notably, this semi-transparent PSC-IZO was sent to Shanghai Institute of Microsystem and Information Technology, Chinese Academy of Science for third party professional organization certification. The ST-PSC measured with PCE of 19.07% (V_{oc} = 1.20 V, J_{sc} = 19.48 mA/cm^2, FF = 81.56%) in house was certified to have a PCE of 18.74% (V_{oc} = 1.199 V, J_{sc} = 18.89 mA/cm^2, FF = 82.89%). As far as we know, this is the highest reported efficiency for wide-bandgap (> 1.65 eV) semi-transparent PSC.

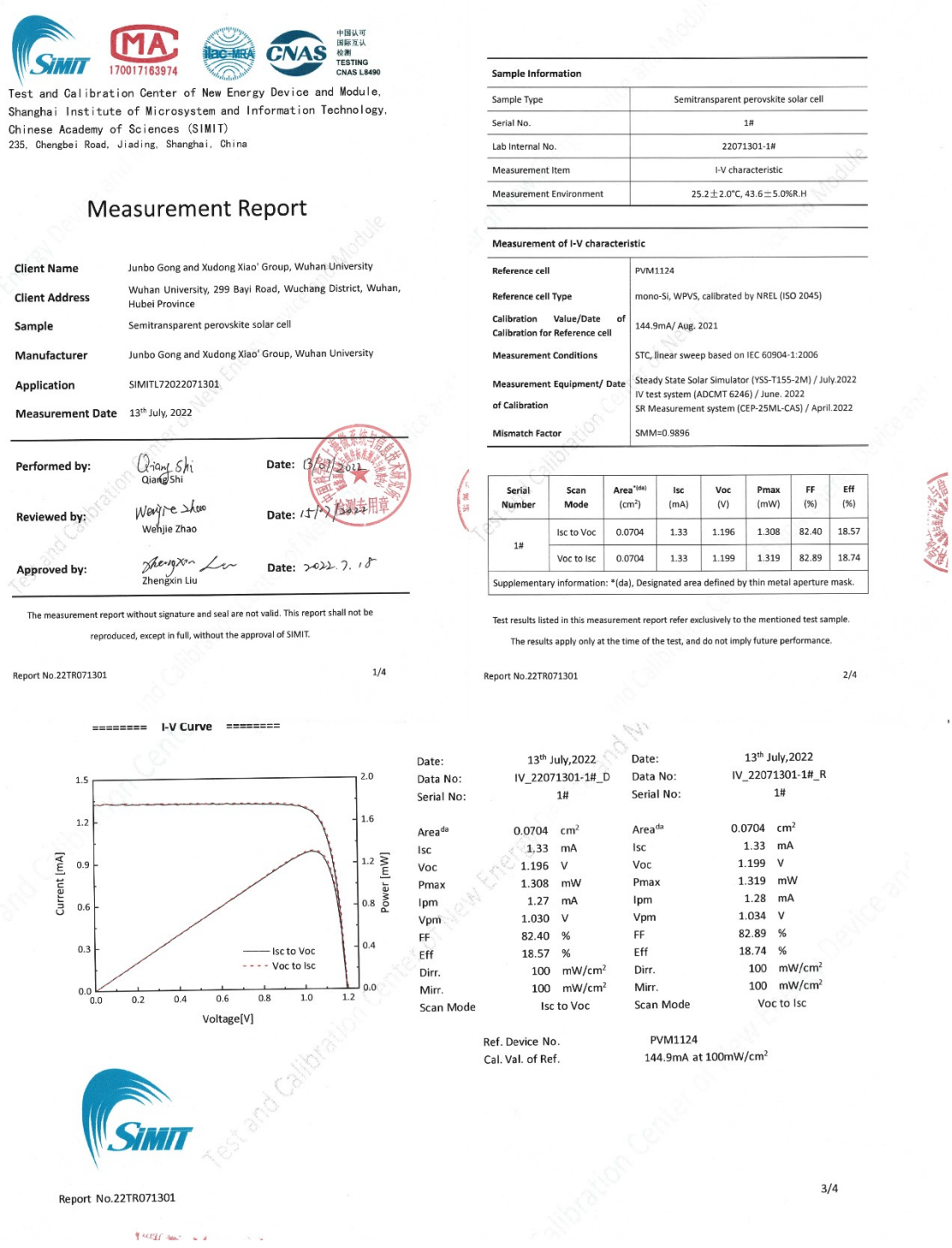

Test and Calibration Center of New Energy Device and Module,
Shanghai Institute of Microsystem and Information Technology,
Chinese Academy of Sciences (SIMIT)
235, Chengbei Road, Jiading, Shanghai, China

Measurement Report

Client Name	Junbo Gong and Xudong Xiao' Group, Wuhan University
Client Address	Wuhan University, 299 Bayi Road, Wuchang District, Wuhan, Hubei Province
Sample	Semitransparent perovskite solar cell
Manufacturer	Junbo Gong and Xudong Xiao' Group, Wuhan University
Application	SIMITL72022071301
Measurement Date	13th July, 2022

Performed by: Qiang Shi Date: 13/07/2022
Reviewed by: Wenjie Zhao Date: 13/07/2022
Approved by: Zhengxin Liu Date: 2022.7.18

The measurement report without signature and seal are not valid. This report shall not be reproduced, except in full, without the approval of SIMIT.

Report No.22TR071301 1/4

Sample Information	
Sample Type	Semitransparent perovskite solar cell
Serial No.	1#
Lab Internal No.	22071301-1#
Measurement Item	I-V characteristic
Measurement Environment	25.2±2.0°C, 43.6±5.0%R.H

Measurement of I-V characteristic	
Reference cell	PVM1124
Reference cell Type	mono-Si, WPVS, calibrated by NREL (ISO 2045)
Calibration Value/Date of Calibration for Reference cell	144.9mA/ Aug. 2021
Measurement Conditions	STC, linear sweep based on IEC 60904-1:2006
Measurement Equipment/ Date of Calibration	Steady State Solar Simulator (YSS-T155-2M) / July.2022 IV test system (ADCMT 6246) / June. 2022 SR Measurement system (CEP-25ML-CAS) / April.2022
Mismatch Factor	SMM=0.9896

Serial Number	Scan Mode	Area*(da) (cm^2)	Isc (mA)	Voc (V)	Pmax (mW)	FF (%)	Eff (%)
1#	Isc to Voc	0.0704	1.33	1.196	1.308	82.40	18.57
	Voc to Isc	0.0704	1.33	1.199	1.319	82.89	18.74

Supplementary information: *(da), Designated area defined by thin metal aperture mask.

Test results listed in this measurement report refer exclusively to the mentioned test sample.
The results apply only at the time of the test, and do not imply future performance.

Report No.22TR071301 2/4

======== I-V Curve ========

Date:	13th July,2022		Date:	13th July,2022
Data No:	IV_22071301-1#_D		Data No:	IV_22071301-1#_R
Serial No:	1#		Serial No:	1#
Area^{da}	0.0704	cm^2	Area^{da}	0.0704 cm^2
Isc	1.33	mA	Isc	1.33 mA
Voc	1.196	V	Voc	1.199 V
Pmax	1.308	mW	Pmax	1.319 mW
Ipm	1.27	mA	Ipm	1.28 mA
Vpm	1.030	V	Vpm	1.034 V
FF	82.40	%	FF	82.89 %
Eff	18.57	%	Eff	18.74 %
Dirr.	100	mW/cm^2	Dirr.	100 mW/cm^2
Mirr.	100	mW/cm^2	Mirr.	100 mW/cm^2
Scan Mode	Isc to Voc		Scan Mode	Voc to Isc

Ref. Device No. PVM1124
Cal. Val. of Ref. 144.9mA at 100mW/cm^2

Report No.22TR071301 3/4

======== **Normalized External Quantum Efficiency Curve** ========

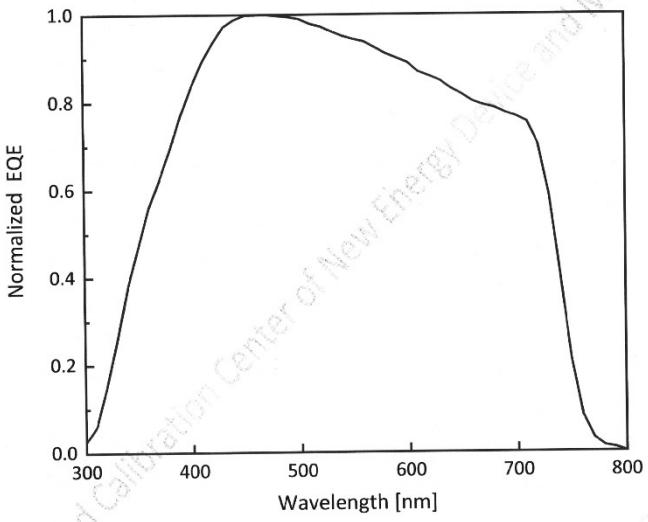

------- End of Report -------

Supplementary Note 3: Certified performance of CIGS device. A CIGS solar cell with house measured PCE of 18.25% (V_{oc} = 0.607 V, J_{sc} = 39.75 mA/cm^2, FF = 75.60%) was certified with a PCE of 18.38% (V_{oc} = 0.606 V, J_{sc} = 39.48 mA/cm^2, FF = 76.87%) by Shanghai Institute of Microsystem and Information Technology, Chinese Academy of Science.

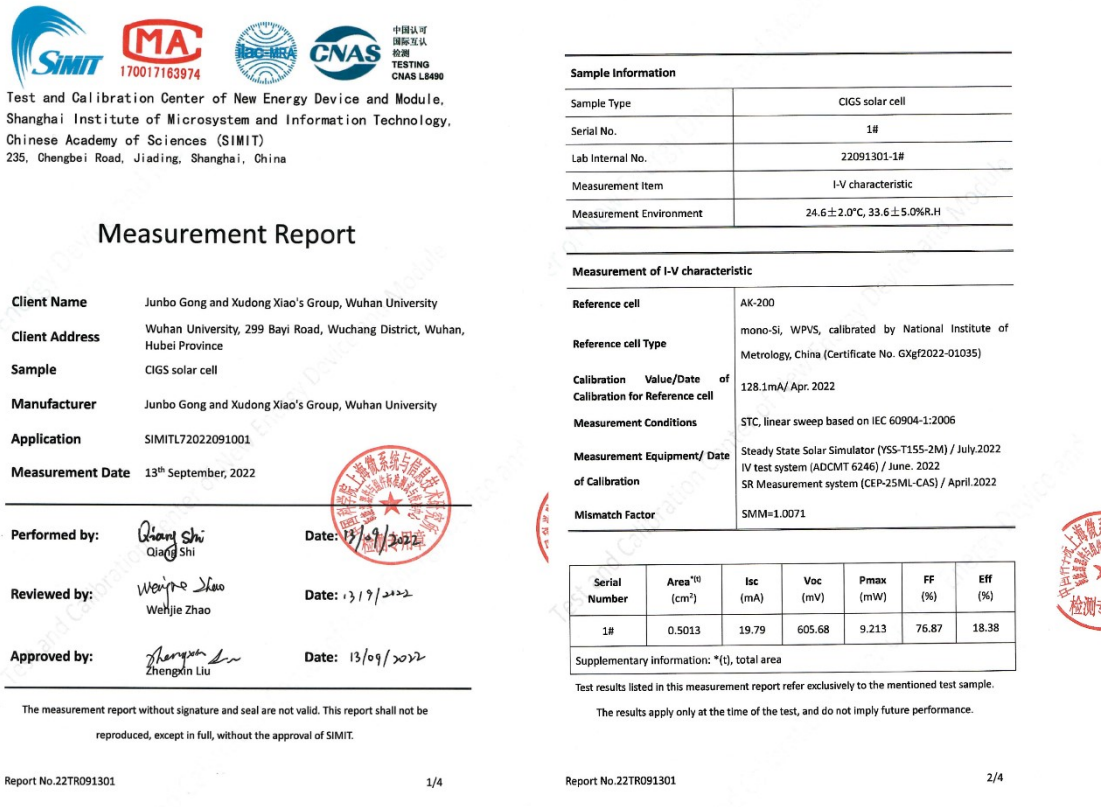

Test and Calibration Center of New Energy Device and Module,
Shanghai Institute of Microsystem and Information Technology,
Chinese Academy of Sciences (SIMIT)
235, Chengbei Road, Jiading, Shanghai, China

Measurement Report

Client Name	Junbo Gong and Xudong Xiao's Group, Wuhan University
Client Address	Wuhan University, 299 Bayi Road, Wuchang District, Wuhan, Hubei Province
Sample	CIGS solar cell
Manufacturer	Junbo Gong and Xudong Xiao's Group, Wuhan University
Application	SIMITL72022091001
Measurement Date	13th September, 2022

Performed by: Qiang Shi — **Date:** 13/09/2022

Reviewed by: Wenjie Zhao — **Date:** 13/9/2022

Approved by: Zhengxin Liu — **Date:** 13/09/2022

The measurement report without signature and seal are not valid. This report shall not be reproduced, except in full, without the approval of SIMIT.

Sample Information

Sample Type	CIGS solar cell
Serial No.	1#
Lab Internal No.	22091301-1#
Measurement Item	I-V characteristic
Measurement Environment	24.6±2.0°C, 33.6±5.0%R.H

Measurement of I-V characteristic

Reference cell	AK-200
Reference cell Type	mono-Si, WPVS, calibrated by National Institute of Metrology, China (Certificate No. GXgf2022-01035)
Calibration Value/Date of Calibration for Reference cell	128.1mA/ Apr. 2022
Measurement Conditions	STC, linear sweep based on IEC 60904-1:2006
Measurement Equipment/ Date of Calibration	Steady State Solar Simulator (YSS-T155-2M) / July.2022 IV test system (ADCMT 6246) / June. 2022 SR Measurement system (CEP-25ML-CAS) / April.2022
Mismatch Factor	SMM=1.0071

Serial Number	Area*(t) (cm^2)	Isc (mA)	Voc (mV)	Pmax (mW)	FF (%)	Eff (%)
1#	0.5013	19.79	605.68	9.213	76.87	18.38

Supplementary information: *(t), total area

Test results listed in this measurement report refer exclusively to the mentioned test sample.

The results apply only at the time of the test, and do not imply future performance.

======== I-V Curve ========

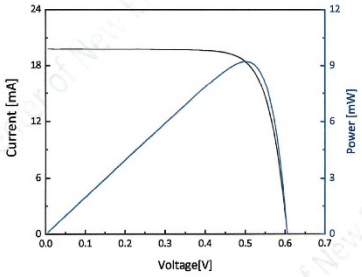

Date:	13th Septemeber,2022	
Data No:	IV_22091301-1#	
Serial No:	1#	
Area¹	0.5013	cm^2
Isc	19.79	mA
Voc	605.68	mV
Pmax	9.213	mW
Ipm	18.38	mA
Vpm	501.27	mV
FF	76.87	%
Eff	18.38	%
Dirr.	100	mW/cm^2
Mirr.	100	mW/cm^2

Ref. Device No	AK-200
Cal. Val. of Ref.	128.1mA at 100mW/cm^2

======== Normalized External Quantum Efficiency Curve ========

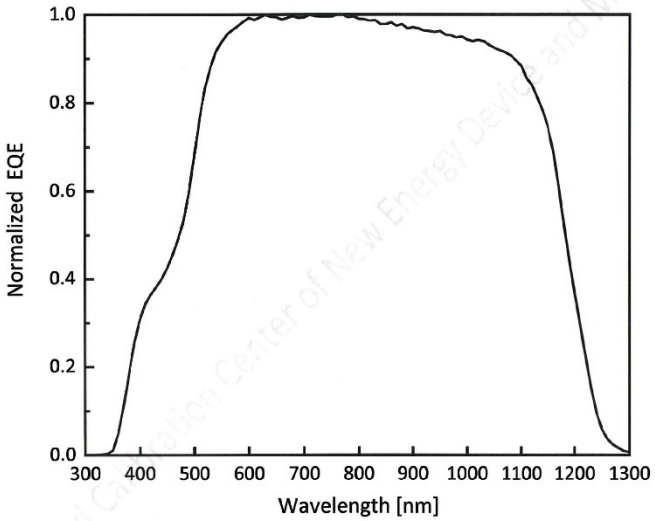

------- End of Report -------

Supplementary Note 4: Certified performance of filtered CIGS device. A filtered CIGS subcell with house measured PCE of 9.30% (V_{oc} = 0.604 V, J_{sc} = 20.33 mA/cm^2, FF = 75.60%) was certified with a PCE of 9.35% (V_{oc} = 0.610 V, J_{sc} = 20.33 mA/cm^2, FF = 75.38%) by Shanghai Institute of Microsystem and Information Technology, Chinese Academy of Science.

中国科学院上海微系统与信息技术研究所
新能源器件与组件标准测试与校准中心
Test and Calibration Center of New Energy Device and Module, Shanghai Institute of Microsystem and Information Technology, Chinese Academy of Sciences (SIMIT)

测 试 报 告
Test Report

报告编号：23TR060104
Report No.

委托单位：Client	Junbo Gong and Xudong Xiao's Group, Wuhan University
单位地址：Client Address	299 Bayi Road, Wuchang District, Wuhan, Hubei Province
检测对象：Sample	Short-circuited Perovskite Filtered CIGS Cell
生产厂家：Manufacture	Junbo Gong and Xudong Xiao's Group, Wuhan University

测试/Performed by: 日期/Date: 2022/06/01
审核/Reviewed by: 日期/Date: 2022/06/01
批准/Approved by: 日期/Date: 2022/06/01

地址：上海市嘉定区城北路 235 号
Address: No.235 Chengbei Road, Jiading, Shanghai
邮编/Post Code:201800
邮箱/E-mail: solarcell@mail.sim.ac.cn
电话/Tel: +86-021-69976921

1 / 4

Report No. 23TR060104

声 明 Statements

1、 检测报告涂改、增删、缺页无效。
This report is invalid if it is altered, added, deleted or missing page.
2、 未经本中心书面同意，不得部分复制（全文复制除外）检测报告。
This report shall not be reproduced, except in full, without the approval of SIMIT.
3、 检测报告无编制人、审核人、授权签字人签字无效。
This report is invalid without the signature of the person who performed, reviewed or approved it.
4、 本报告未加盖中心公章和骑缝章无效。
This report is invalid without seal and cross stitch seal.
5、 如对本检测报告内容有异议，应于收到检测报告之日起 15 天内向我单位提出书面意见，否则视作对本报告无异议。
If any objection to the content of this report, please put forward written requirement to our company within 15 days from the date of receiving this report, otherwise it will be deemed that you have no objection to this report.
6、 本声明有中英文两种语言，如有任何分歧，以中文语言为准。
This statement is made in both Chinese and English. In case of any discrepancy, the Chinese language will prevail.
7、 未经本中心同意，任何单位和个人不得以本中心名义和本检测报告作商业广告。
Without the approval of SIMIT, no unit or individual may make commercial advertisements in the name of the center and the test report.
8、 凡伪造本中心检测报告，作虚假广告，本中心将追究法律责任。
Anyone who falsifies the test report of the center and makes false advertisements will be investigated for legal responsibility by SIMIT.

2 / 4

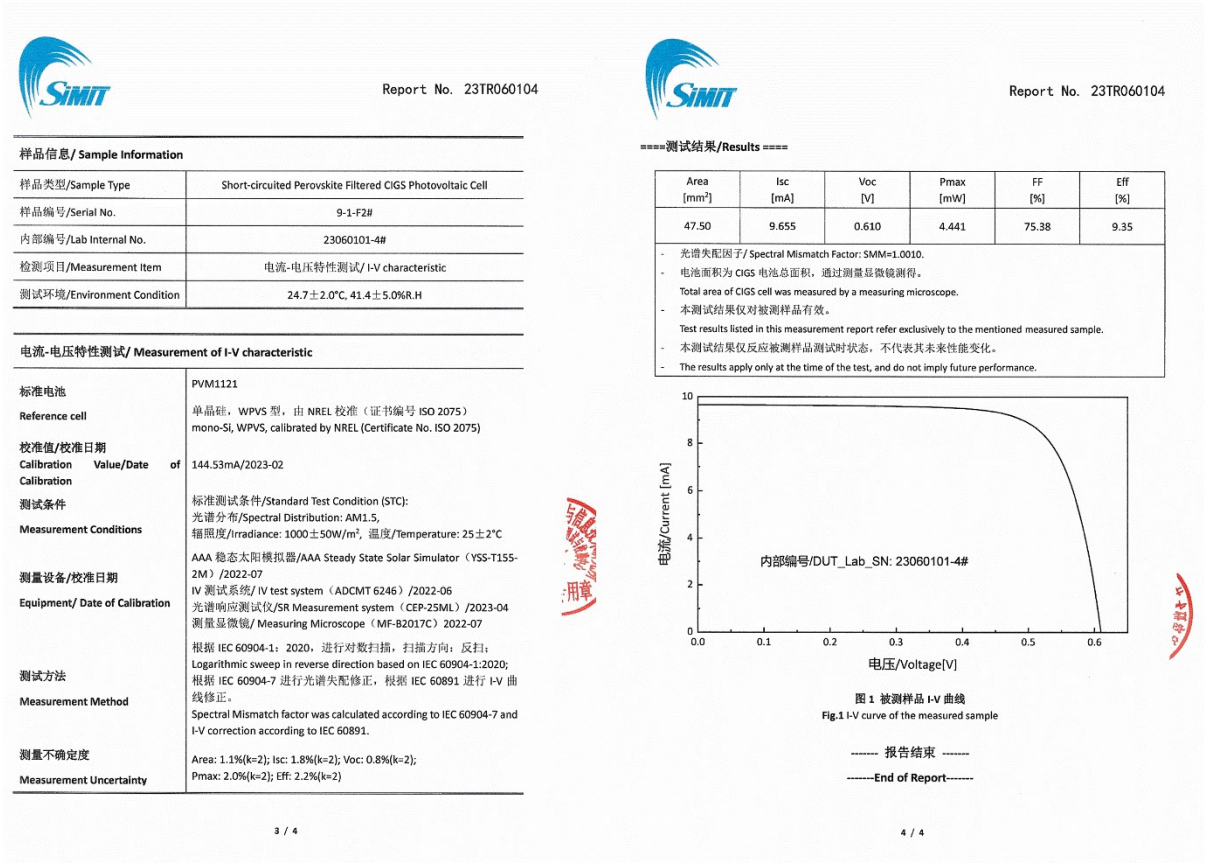

Report No. 23TR060104

样品信息/ Sample Information

样品类型/Sample Type	Short-circuited Perovskite Filtered CIGS Photovoltaic Cell
样品编号/Serial No.	9-1-F2#
内部编号/Lab Internal No.	23060101-4#
检测项目/Measurement Item	电流-电压特性测试/ I-V characteristic
测试环境/Environment Condition	24.7±2.0°C, 41.4±5.0%R.H

电流-电压特性测试/ Measurement of I-V characteristic

标准电池 Reference cell	PVM1121 单晶硅，WPVS 型，由 NREL 校准（证书编号 ISO 2075） mono-Si, WPVS, calibrated by NREL (Certificate No. ISO 2075)
校准值/校准日期 Calibration Value/Date of Calibration	144.53mA/2023-02
测试条件 Measurement Conditions	标准测试条件/Standard Test Condition (STC): 光谱分布/Spectral Distribution: AM1.5, 辐照度/Irradiance: 1000±50W/m², 温度/Temperature: 25±2°C
测量设备/校准日期 Equipment/ Date of Calibration	AAA 稳态太阳模拟器/AAA Steady State Solar Simulator（YSS-T155-2M）/2022-07 IV 测试系统/ IV test system（ADCMT 6246）/2022-06 光谱响应测试仪/SR Measurement system（CEP-25ML）/2023-04 测量显微镜/ Measuring Microscope（MF-B2017C）2022-07
测试方法 Measurement Method	根据 IEC 60904-1：2020，进行对数扫描，扫描方向：反扫； Logarithmic sweep in reverse direction based on IEC 60904-1:2020; 根据 IEC 60904-7 进行光谱失配修正，根据 IEC 60891 进行 I-V 曲线修正。 Spectral Mismatch factor was calculated according to IEC 60904-7 and I-V correction according to IEC 60891.
测量不确定度 Measurement Uncertainty	Area: 1.1%(k=2); Isc: 1.8%(k=2); Voc: 0.8%(k=2); Pmax: 2.0%(k=2); Eff: 2.2%(k=2)

3 / 4

Report No. 23TR060104

====测试结果/Results ====

Area [mm²]	Isc [mA]	Voc [V]	Pmax [mW]	FF [%]	Eff [%]
47.50	9.655	0.610	4.441	75.38	9.35

- 光谱失配因子/ Spectral Mismatch Factor: SMM=1.0010.
- 电池面积为 CIGS 电池总面积，通过测量显微镜测得。
  Total area of CIGS cell was measured by a measuring microscope.
- 本测试结果仅对被测样品有效。
  Test results listed in this measurement report refer exclusively to the mentioned measured sample.
- 本测试结果仅反应被测样品测试时状态，不代表其未来性能变化。
- The results apply only at the time of the test, and do not imply future performance.

图 1 被测样品 I-V 曲线
Fig.1 I-V curve of the measured sample

------- 报告结束 -------
-------End of Report-------

4 / 4

Supplementary Note 5:

Suppression of J_{sc} by PDI surface treatment and its recovery in Cl+PDI samples

A side story is about the current decrease in **PDI** devices, this requires information on the band alignments and work functions. To explore the effect on band alignment by the Cl incorporation and the PDI treatment, the energy levels of the four groups of perovskite films were measured by ultraviolet photoelectron spectroscopy (UPS). The obtained spectra and the corresponding schematics of the energy band edge positions were shown in Supplementary Fig. 14. As observed, with respect to the Fermi level, the Cl incorporation caused a slight upward shift of ~ 50 meV for both the conduction and valence band while the PDI treatment led to a downward shift of ~ 120 meV for both bands. For the **Cl + PDI** group samples, their conduction and valence band edges were located between those of **PDI** and **Cl** groups but were slightly lower than those of the **Control** group samples. According to the Anderson rule by

keeping the Fermi level constant along the entire solar cell structure, the band bending in the devices could be constructed as shown in Supplementary Fig. 15. It was important to note that the PDI treatment primarily affected the surface of the perovskite films. Adding such a thin PDI treated layer would effectively make the transport of both electrons and holes between the bulk absorber and the ETL layer smoother if only the conduction and valence band edge positions were considered. However, once the alignment of vacuum levels was examined, interesting features occurred. For the **PDI** sample, considering that the thin PDI treated layer had a relative higher work function than that of the bulk absorber (same as that of **Control** sample, Supplementary Fig. 15) by ~210 meV, there would result in an interfacial electric diploe field with a direction running from the bulk absorber to the PDI treated layer.[16] This electric field formed an energy barrier of ~210 meV in magnitude with the conduction band bending upwards for electron transport from bulk absorber to the PDI treated surface. This energy barrier was presumably responsible for the observed *Jsc* decrease of the corresponding device as also discussed in literature.[17] In contrast, the work functions of the **Cl** and **Cl + PDI** samples were similar to that of **Control** sample and no barrier was expected to form for the electron transport, thus the resultant *Jsc* was comparable among the corresponding devices. In particular, the work function of the **Cl + PDI** surface layer was even reduced from that of **Cl** sample by ~ 80 meV, leading to a descending order of vacuum level from the Cl incorporated absorber layer to the **Cl +PDI** surface layer and to the ETL layer. The consequently formed electric fields at both Cl/Cl+PDI and Cl+PDI/ETL interfaces resulted in downward band bending and were along the right direction to promote electron and hole transport (Supplementary Fig. 15). In this way, the observed significant decrease of J_{sc} in **PDI** samples was well explained by the large work function of PDI treated layer.

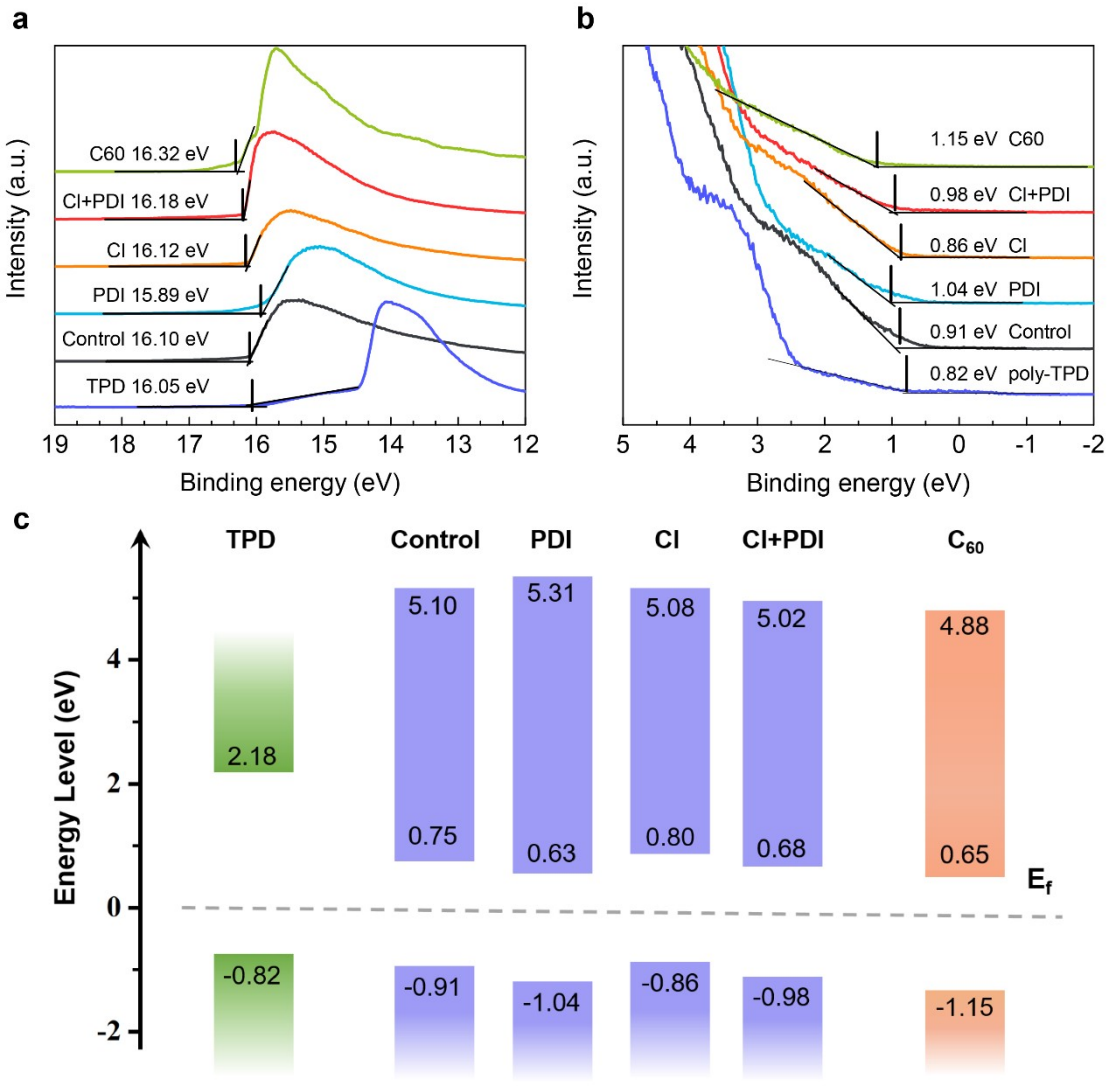

Supplementary Figure 14. UPS results and energy levels. a-b, UPS spectra of representative perovskite films from the four groups. The light source is He-I with photon energy of 21.2 eV. **c**, The work function and the conduction and valence band edge positions with respect to the Fermi level for **Control**, **PDI**, **Cl**, **Cl + PDI** samples determined by UPS spectra. The conduction band minima are calculated from the valence band maxima with the bandgap values for perovskite films obtained in Suppl. Fig 1f and for C_{60} and TPD taken from Refs.[18, 19].

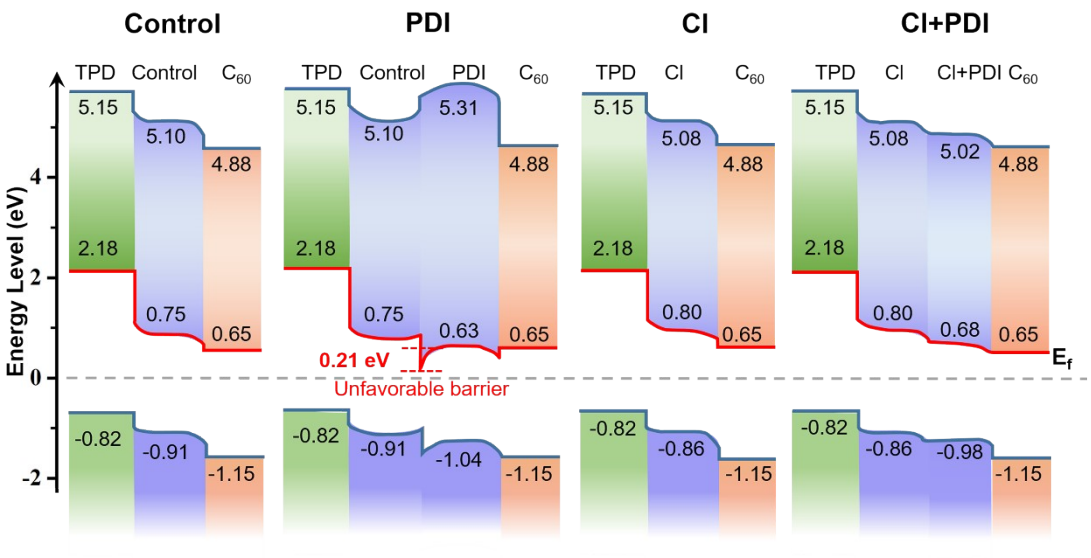

Supplementary Figure 15. Band alignment and band bending. Energy level diagram for **Control**, **PDI**, **Cl**, **Cl + PDI** devices constructed in accordance to the Anderson rule. The width of each layer is not in scale with the real material. Due to the work function difference, there forms an energy barrier of ~210 meV for electron transport from bulk perovskite to PDI treated surface in the case of **PDI** device.

Fortunately, the PDI treatment on the Cl incorporated absorber surface did not generate such an energy barrier and the beneficial effect of surface defect passivation by PDI was realized for V_{oc} without sacrificing J_{sc}. To further investigate why the **PDI** sample possessed a relatively high work function, high-resolution X-ray photoelectron spectroscopy (XPS) was performed. As shown in Supplementary Fig. 16, the C 1s binding energies at 284.8, 286.8, 288.2 eV were assigned respectively to the C-C bond (from FA and PDI), the characteristic peak of PDI, and the C=O. Oxidized carbon species might originate from the oxidation of the perovskite films when exposed to ambient environment before measurement. Interestingly, the peak area of C=O showed a visible decrease after either PDI treatment or Cl incorporation, implying a suppressed oxidization and improved film stability by the according treatments. The

peaks appearing at around 286.8 eV in the C 1s spectra (Supplementary Fig. 16a) and 402.3 eV in the N 1s spectra (Supplementary Fig. 16b) were attributed to the C-N bonds in the six-membered ring of PDI, which clearly verified the existence of PDI. The featured bond of C-N(FA) slightly shifted to higher binding energies after either PDI treatment or Cl incorporation. This shift may originate from the interaction between FA^+ and $R_2NH_2^+$ from PDI. In the Pb 4f spectra shown in Supplementary Fig. 16c, the binding energies at 143.1 and 138.3 eV were assigned to $4f_{5/2}$ and $4f_{7/2}$ of divalent Pb^{2+}, respectively. These peaks slightly moved to higher binding energy only after Cl incorporation in terms of bond formation of Pb-Cl. From Supplementary Fig. 16 and in Supplementary Table 3，after PDI treatment, we observed an increased signal of C-C (FA+PDI) by ~26-31% due to the increased C density in PDI against perovskite, a decreased signal of Pb 4f by ~12-20% due to the absence of Pb in the PDI layer. The above increase of C 1s signal and decrease of Pb 4f signal are consistent with a ~ 2 nm PDI layer covered on the perovskite film even taking into account of electron energy dependent attenuation length, but the strongly decreased N 1s (FA) signal by ~35-38% indicated a net drop of N-C (FA) signal beyond the attenuation effect (~21%). Thus, PDI molecules would occupy some vacancies of the FA^+ ions at the surface of perovskite films. Compared to the original surface, the replacement of FA^+ by neutral PDI molecules and the filling of V_I^+ vacancies by neutral PDI molecules might effectively make the surface more charge negative, leading to the formation of an effective electric dipole layer pointing towards the bulk of perovskite layer. This effective electric dipole layer was suggested to induce the observed work function increase in the **PDI** samples.

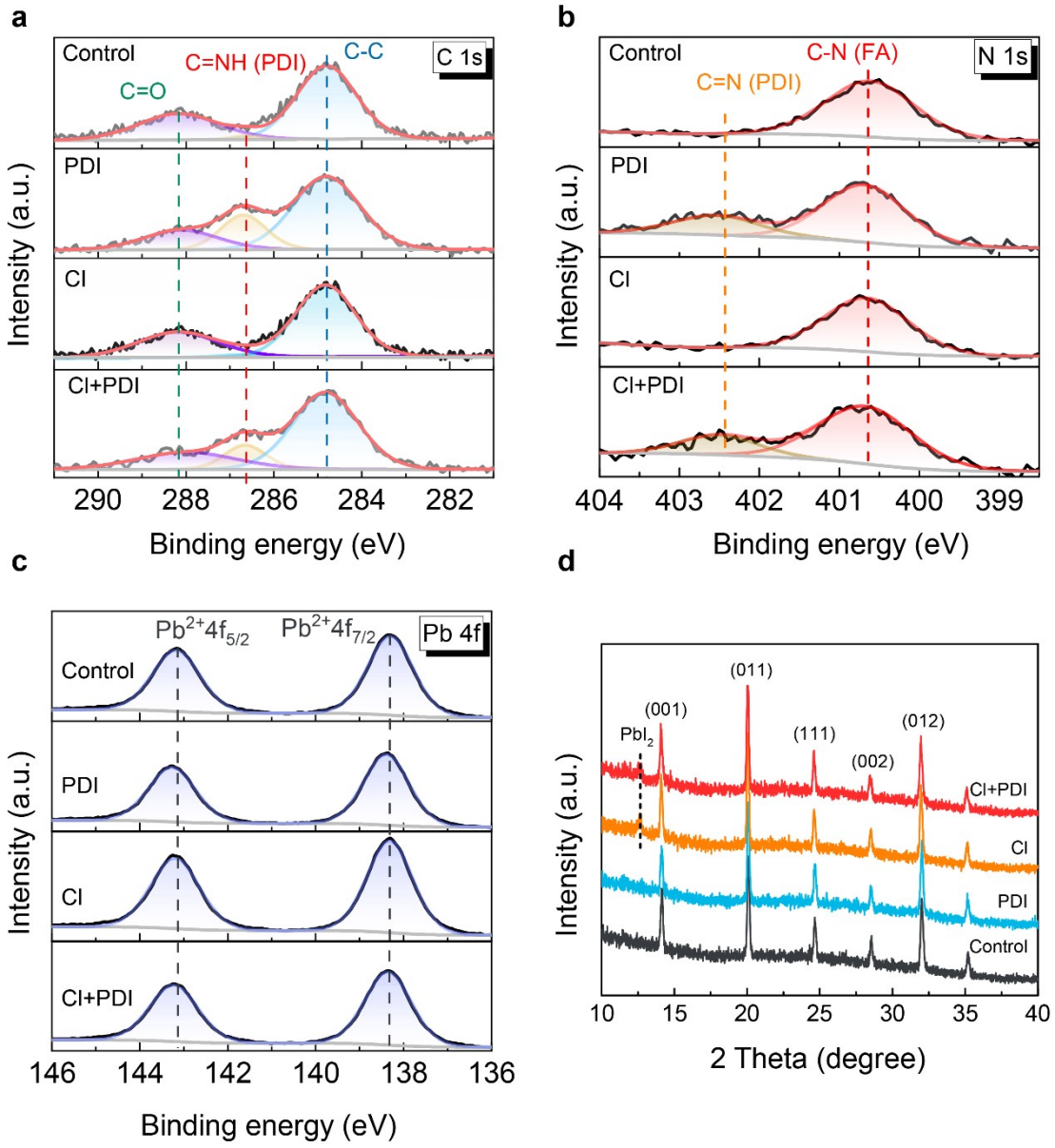

Supplementary Figure 16. High-resolution XPS and XRD spectra of perovskite films. a, C 1s XPS spectra, **b**, N 1s XPS spectra, **c**, Pb 4f XPS spectra, **d**, XRD patterns.

Supplementary Table 3. Peak area of corresponding XPS spectra.

	C-C (FA+PDI)	N-C (FA)	$Pb^{2+}4f_{5/2}$
Control	10213	9031	51769
PDI	12880	5620	45728
Cl	9382	7291	60944
Cl + PDI	12332	4708	48604

While the above picture could well explain the work function increase for **PDI** samples, it encountered difficulty with the **Cl+PDI** samples. To identify the role of Cl incorporation, the fabricated perovskite films was further studied by XRD. As shown in Supplementary Fig. 16d, the XRD peak at 12.6° revealed the existence of PbI_2 phase in the **Cl** and **Cl + PDI** samples in contrast to its absence in the **Control** and **PDI** samples. Although no excessive PbI_2 was used in the precursors, the formation of PbI_2 trace phase on the surface of perovskite containing Cl, as also observed by other groups,[6, 21] seemed to imply that species such as $FAPb(I_2Cl)$ might decompose into PbI_2 and FACl, and the latter might be vaporized away to leave only PbI_2 on the surface.

Our previous work[22] as well as others' work[6, 21, 23] have shown that a small amount of PbI_2 on the surface was beneficial to passivate defects at grain boundaries and surfaces and thus helped the improvement of device performance. We speculated that PbI_2 might in addition play a role on regulating the work function of perovskite surface layer. Considering that iodine deficiencies are highly likely to exist in the remnant PbI_2 layer on perovskite,[24] these iodine deficiencies with positive effective positive charge, V_I^+, should result in the formation of an effective electric dipole layer pointing towards the surface of perovskite layer, which was opposite to the dipole direction formed on the surface of **PDI** samples and could be responsible for the observed work function decrease in the **Cl** and **Cl+PDI** samples. On the whole, it was possible that the effective charges induced by PbI_2, to reduce the work function, and by PDI, to increase the work function, would neutralize to certain extent and the work functions **Cl + PDI** samples could become lower than that of **PDI** samples.

References:

1. F. Li, X. Deng, F. Qi, Z. Li, D. Liu, D. Shen, M. Qin, S. Wu, F. Lin and S.-H. Jang, *J. Am. Chem. Soc.* 2020, **142**, 20134-20142.
2. T. Duong, Y. Wu, H. Shen, J. Peng, X. Fu, D. Jacobs, E. C. Wang, T. C. Kho, K. C. Fong and M. Stocks, *Adv. Energy Mater.* 2017, **7**, 1700228.
3. C. O. R. Quiroz, Y. Shen, M. Salvador, K. Forberich, N. Schrenker, G. D. Spyropoulos, T. Heumüller, B. Wilkinson, T. Kirchartz and E. Spiecker, *J. Mater. Chem. A* 2018, **6**, 10149-10149.
4. M. Jaysankar, B. A. Raul, J. Bastos, C. Burgess, C. Weijtens, M. Creatore, T. Aernouts, Y. Kuang, R. Gehlhaar and A. Hadipour, *ACS Energy Lett.* 2018, **4**, 259-264. *ACS Energy Lett.* **4**, 259-264 (2018).
5. Kim, D.H. et al. Bimolecular additives improve wide-band-gap perovskites for efficient tandem solar cells with CIGS. *Joule* **3**, 1734-1745 (2019).
6. J. Xu, C. C. Boyd, Z. J. Yu, A. F. Palmstrom, D. J. Witter, B. W. Larson, R. M. France, J. Werner, S. P. Harvey and E. J. Wolf, *Science* 2020, **367**, 1097-1104.
7. T. Duong, H. Pham, T. C. Kho, P. Phang, K. C. Fong, D. Yan, Y. Yin, J. Peng, M. A. Mahmud and S. Gharibzadeh, *Adv. Energy Mater.* 2020, **10**, 1903553.
8. E. Aydin, M. De Bastiani, X. Yang, M. Sajjad, F. Aljamaan, Y. Smirnov, M. N. Hedhili, W. Liu, T. G. Allen and L. Xu, *Adv. Funct. Mater.* 2019, **29**, 1901741.
9. B. Chen, S.-W. Baek, Y. Hou, E. Aydin, M. De Bastiani, B. Scheffel, A. Proppe, Z. Huang, M. Wei and Y.-K. Wang, *Nat. Commun.* 2020, **11**, 1257.
10. Z. Wang, X. Zhu, S. Zuo, M. Chen, C. Zhang, C. Wang, X. Ren, Z. Yang, Z. Liu and X. Xu, *Adv. Funct. Mater.* 2020, **30**, 1908298.
11. D. Yang, X. Zhang, Y. Hou, K. Wang, T. Ye, J. Yoon, C. Wu, M. Sanghadasa, S. F. Liu and S. Priya, *Nano Energy*, 2021, **84**, 105934.
12. C. Wang, Y. Zhao, T. Ma, Y. An, R. He, J. Zhu, C. Chen, S. Ren, F. Fu and D. Zhao, *Nat. Energy* 2022, **7**, 744-753.
13. Y. Yao, P. Hang, B. Li, Z. Hu, C. Kan, J. Xie, Y. Wang, Y. Zhang, D. Yang and X. Yu, *Small*, 2022, **18**, 2203319.
14. L. Yan, S. Qiu, B. Yu, J. Huang, J. Qiu, C. Zhang, F. Guo, Y. Yang and Y. Mai, *Advanced Energy and Sustainability Research* 2022, **3**, 2100199.
15. G. S. Jang, Y. Kim, Y. Y. Kim, J. J. Yoo, G. Kim, N. J. Jeon, H.-S. Lee, D. Kim and J. Seo, *Sol. RRL* 2022, **6**, 2200252.
16. M. A. Martínez-Puente, J. Tirado, F. Jaramillo, R. Garza-Hernández, P. Horley, L. G. Silva Vidaurri, F. S. Aguirre-Tostado and E. Martinez-Guerra, *ACS Appl. Energ. Mater.* 2021, **4**, 10896-10908.
17. X. Zhuang, R. Sun, D. Zhou, S. Liu, Y. Wu, Z. Shi, Y. Zhang, B. Liu, C. Chen and D. Liu, *Adv. Funct. Mater.* 2022, **32**, 2110346.
18. C. Liu, Y. Yang, C. Zhang, S. Wu, L. Wei, F. Guo, G. M. Arumugam, J. Hu, X. Liu and J. Lin, *Adv. Mater.* 2020, **32**, 1907361.
19. Z. Xiao, R. A. Kerner, L. Zhao, N. L. Tran, K. M. Lee, T.-W. Koh, G. D. Scholes and B. P. Rand, *Nat. Photonics* 2017, **11**, 108-115. *Nat. Photonics* **11**, 108-115 (2017).
20. J. Yang, S. Xiong, J. Song, H. Wu, Y. Zeng, L. Lu, K. Shen, T. Hao, Z. Ma and F. Liu, *Adv. Energy Mater.* 2020, **10**, 2000687.
21. F. Jiang, Y. Rong, H. Liu, T. Liu, L. Mao, W. Meng, F. Qin, Y. Jiang, B. Luo and S. Xiong, *Adv. Funct. Mater.* 2016, **26**, 8119-8127.
22. X. Liu, Z. Wu, X. Fu, L. Tang, J. Li, J. Gong and X. Xiao, *Nano Energy*, 2021, **86**, 106114.
23. J. Euvrard, O. Gunawan and D. B. Mitzi, *Adv. Energy Mater.* 2019, **9**, 1902706.

24. H. Chen, H. Yan and Y. Cai, *Chem. Mat.* 2022, **34**, 1020-1029.